PHYSICAL REVIEW B **89**, 014426 (2014)

Complex magnetic behavior of the sawtooth Fe chains in $Rb_2Fe_2O(AsO_4)_2$

V. Ovidiu Garlea,[1,*] Liurukara D. Sanjeewa,[2] Michael A. McGuire,[3] Pramod Kumar,[4] Dino Sulejmanovic,[2]
Jian He,[5] and Shiou-Jyh Hwu[2]

[1]*Quantum Condensed Matter Division, Oak Ridge National Laboratory, Oak Ridge, Tennessee 37831, USA*
[2]*Department of Chemistry, Clemson University, Clemson, South Carolina 29634-0973, USA*
[3]*Materials Science and Technology Division, Oak Ridge National Laboratory, Oak Ridge, Tennessee 37831, USA*
[4]*Indian Institute of Information Technology, Allahabad U.P. 211012, India*
[5]*Department of Physics and Astronomy, Clemson University, Clemson, South Carolina 29634-0978, USA*

(Received 4 December 2013; published 29 January 2014)

Results of magnetic field and temperature-dependent neutron-diffraction and magnetization measurements on oxy-arsenate $Rb_2Fe_2O(AsO_4)_2$ are reported. The crystal structure of this compound contains pseudo-one-dimensional $[Fe_2O_6]^\infty$ sawtoothlike chains, formed by corner-sharing isosceles triangles of Fe^{3+} ions occupying two nonequivalent crystallographic sites. The chains extend infinitely along the crystallographic b axis and are structurally confined from one another via diamagnetic $(AsO_4)^{3-}$ units along the a axis and Rb^+ cations along the c-axis direction. Neutron-diffraction measurements indicate the onset of a long-range antiferromagnetic order below approximately 25 K. The magnetic structure consists of ferrimagnetic chains which are antiferromagnetically coupled with each other. Within each chain, one of the two Fe sites carries a moment which lies along the b axis, while the second site bears a canted moment in the opposite direction. Externally applied magnetic field induces a transition to a ferrimagnetic state, in which the coupling between the sawtooth chains becomes ferromagnetic. Magnetization measurements performed on optically aligned single crystals reveal evidence for an uncompensated magnetization at low magnetic fields that could emerge from a phase-segregated state with ferrimagnetic inclusions or from antiferromagnetic domain walls. The observed magnetic states and the competition between them are expected to arise from strongly frustrated interactions within the sawtooth chains and relatively weak coupling between them.

DOI: 10.1103/PhysRevB.89.014426 PACS number(s): 75.50.Gg, 75.60.Jk, 75.25.−j, 71.27.+a

I. INTRODUCTION

Low-dimensional magnetic materials have drawn continued attention in condensed matter physics, owing to their distinct electronic and magnetic properties. In particular, the oxyanion systems based on transition-metal (M) oxide sublattices that are magnetically isolated by closed-shell nonmagnetic oxyanions (SiO_4^{4-}, PO_4^{3-}, AsO_4^{3-}) show great potential for exploring and characterizing new emergent phenomena [1]. This class of compounds has been shown to exhibit a variety of magnetic ground states ranging from ferromagnetism to ferrimagnetism and antiferromagnetism [2]. On the other hand, due to their impressive structural diversity in terms of architecture, these materials have shown potential applications in the fields of energy storage, chemical sensors, catalysis, and biomedical research [3–6].

Recent efforts have been directed towards the synthesis of new members of the family of oxy-arsenates with general formula $A_2M_2O(AsO_4)_2$, where A = K, Rb, and M is a transition metal. These compounds exhibit intriguing one-dimensional triangular-shaped chains made of edge-sharing MO_6 octahedra (see Fig. 1). The antiferromagnetic sawtooth chain model (or Δ chain), as realized in these systems, is known to be highly frustrated and has drawn considerable attention from a theoretical standpoint [7–9]. For example, the ground state of the $S = 1/2$ sawtooth chain is twofold degenerate with either the left pair or right pair of spin at each triangle forming spin-singlet states. The lowest excitation in a chain with periodic boundary conditions is given by a *kink-antikink* pair, which has a dispersionless gap $\Delta E \simeq 0.234J$ where J is the coupling between pairs of spins [7,8]. The experimental realization of magnetic lattices corresponding to the sawtooth chain is only found in a very small number of compounds, including the delafossite $YCuO_{2.5}$ [10], euchroite $Cu_2(AsO_4)(OH)\cdot 3H_2O$ [11], and ZnL_2S_4 olivines, with L = Er, Tm, Yb [12].

We report here on the magnetic behavior of oxy-arsenite $Rb_2Fe_2O(AsO_4)_2$, containing sawtooth chains of magnetic Fe^{3+} ions in high-spin state $S = 5/2$. Although this compound was first reported five years ago [13], a thorough investigation of its magnetic properties has not been conducted so far. The development of well-controlled methods for the growth of high-quality single crystals has made possible detailed orientation-dependent magnetic measurements. Magnetization measurements have been complemented with x-ray and neutron-diffraction measurements. Temperature- and magnetic-field-dependent neutron-diffraction measurements demonstrate conclusively the development of a noncollinear antiferromagnetic ground state below approximately 25 K, which under relatively low magnetic fields transforms to a ferrimagnetic state. These transitions are also observed in dc magnetization measurements, which reveal strong magnetic anisotropy and complex field- and temperature-dependent behaviors associated with the multiple magnetic states.

II. EXPERIMENTAL DETAILS

Single crystals of $Rb_2Fe_2O(AsO_4)_2$ were grown using flux methods in the RbCl/RbI (50:50 wt%) molten-salt media.

---

[*] garleao@ornl.gov

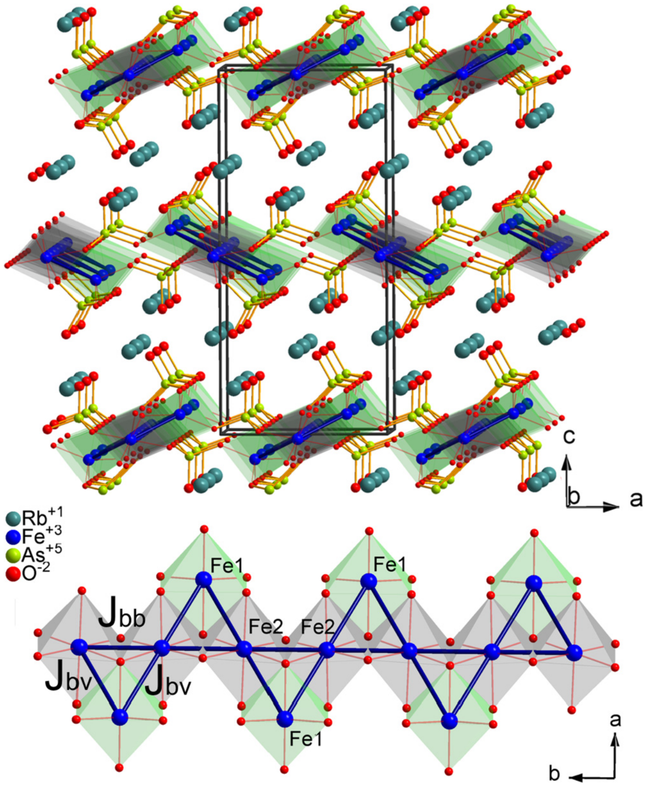

FIG. 1. (Color online) Top: Polyhedral view of the extended structure of $Rb_2Fe_2O(AsO_4)_2$ showing the structural confinement of the chains. Bottom: Partial structure of the $[Fe_4O_{14}]^\infty$ sawtooth chain defined by unequal base-base (J_{bb}) and base-vertex (J_{bv}) exchange interactions.

The reactants KO_2 (Alfa Aesar, 96.5%), Fe_2O_3 (Alfa Aesar, 99.945%), and As_2O_5 (Alfa Aesar, 99.9%) were mixed and ground together in a nitrogen-purged dry box. The reaction mixture was sealed in an evacuated fused-silica ampoule and then heated to 650 °C for one day, followed by another heating to 800 °C at 1 °C/min for two days, slowly cooled to 300 °C at 0.05 °C/min, and then furnace cooled to room temperature. Brown columnar crystals (up to about 2.6 × 0.6 × 0.4 mm) were recovered by washing the product with deionized water using vacuum filtration method. Single crystals were physically examined and selected under an optical microscope equipped with a polarizing light attachment. The crystals were then mounted on a glass fiber and single-crystal x-ray diffraction data were collected using a Rigaku Mercury CCD detector on an AFC-8S diffractometer equipped with graphite monochromated Mo Kα radiation ($\lambda = 0.7107$ Å). The structure was solved by direct methods using the SHELX-97 [14] program and refined on F^2 by the least-squares, full-matrix technique.

Polycrystalline samples were prepared by the solid-state reaction of stoichiometric amounts of Rb_2CO_3 (Alfa Aesar, 99.8%), Fe_2O_3 (Alfa Aesar, 99.945%), and $(NH_4)H_2AsO_4$ (Alfa Aesar, 99.9%). The mixture was loaded into an alumina crucible, heated to 800 °C at a rate of 2 °C/min, and held at that temperature for two days before being furnace cooled to room temperature. All polycrystalline samples were characterized using the Rigaku Ultima IV multipurpose x-ray diffraction system.

Temperature- and field-dependent magnetic measurements were carried out with a Quantum Design Magnetic Property Measurement System (MPMS). The measurements were taken on collections of optically coaligned single crystals at temperatures from 2 to 300 K in the applied fields up to 50 kOe. Additional magnetization measurements were performed on a polycrystalline sample using a physical property measurement system (PPMS) at fields up to 120 kOe.

Neutron-diffraction measurements were carried out using the HB2A high-resolution powder diffractometer at the High Flux Isotope Reactor (HFIR). Diffraction patterns were collected using the 2.408 Å wavelength produced by the (113) reflection of a vertically focusing germanium wafer-stack monochromator. The beam collimation was 12′–40′–6′. More details about the HB2-A instrument and data-collection strategies can be found in Ref. [15]. For the measurements, polycrystalline samples with a total mass of approximately five grams were compacted in pellets to prevent grain reorientation by the applied field. The pellets were loaded into a cylindrical vanadium can and placed in a vertical-field cryomagnet. Data were collected at various temperatures from 40 K down to 4 K, and magnetic fields up to 40 kOe. Rietveld refinements were carried out with the FullProf SUITE program [16].

III. RESULTS AND DISCUSSION

A. Crystal structure

The single-crystal x-ray and neutron powder diffraction data were well fit by using an orthorhombic structure of space group *Pnma*, similar to that proposed by Chang *et al.* [13]. The refined structural parameters of $Rb_2Fe_2O(AsO_4)_2$, such as atomic coordinates and displacement parameters, are listed in Table I, while selected bond lengths and angles are given in Table II. Rietveld analysis indicates that the powder samples contain a Fe_2O_3 impurity phase in an amount of less than 3% weight.

The structure of $Rb_2Fe_2O(AsO_4)_2$ consists of iron-arsenate layers parallel to the *ab* plane, separated by Rb^+ cations. In

TABLE I. Refined structural parameters of $Rb_2Fe_2O(AsO_4)_2$ from single-crystal x-ray data collected at room temperature.

Atom (Wyck.)	x	y	z	U_{eq}
Rb1 (4*c*)	0.8888(1)	1/4	0.8628(1)	0.023(1)
Rb2 (4*c*)	0.0379(1)	1/4	0.2679(1)	0.028(1)
Fe1 (4*c*)	0.2844(1)	1/4	0.4347(1)	0.009(1)
Fe2 (4*b*)	0	0	1/2	0.009(1)
As1 (4*c*)	0.8204(1)	1/4	0.6426(2)	0.010(1)
As2 (4*c*)	0.6758(1)	1/4	0.4440(2)	0.008(1)
O1 (4*c*)	1.0580(1)	1/4	0.4375(3)	0.009(1)
O2 (4*c*)	0.9610(1)	1/4	0.5760(3)	0.010(1)
O3 (8*d*)	0.7666(1)	0.0108(1)	0.4785(2)	0.015(1)
O4 (4*c*)	0.4923(1)	1/4	0.4744(4)	0.014(1)
O5 (8*d*)	0.7043(1)	0.0127(1)	0.6338(2)	0.018(1)
O6 (4*c*)	0.6843(1)	1/4	0.3556(3)	0.018(1)
O7 (4*c*)	0.9130(2)	1/4	0.7197(3)	0.025(1)

Pnma, $a = 8.5331(2)$ Å, $b = 5.7892(2)$ Å, $c = 18.611(4)$ Å
$R_1 = 0.0347$, $wR_2 = 0.0936$, GOF = 1.038

TABLE II. Selected bond distances and angles in $Rb_2Fe_2O(AsO_4)_2$, as determined from x-ray analysis.

Fe1-O1 (×1)	1.932(6) Å	Fe2-O1 (×2)	1.922(4) Å
Fe1-O3 (×2)	2.254(4) Å	Fe2-O2 (×2)	2.051(4) Å
Fe1-O4 (×1)	1.923(6) Å	Fe2-O3 (×2)	2.032(4) Å
Fe1-O5 (×2)	1.986(4) Å		
d(Fe1-Fe2) = 3.076(1) Å⇔ J_{bv} via O1, O3			
Fe1-O3-Fe2 = 91.5(1)°		Fe1-O1-Fe2 =105.9(1)°	
d(Fe2-Fe2) = 2.895(1) Å⇔ J_{bb} via O1, O2			
Fe2-O1-Fe2 = 97.7(1)°		Fe2-O2-Fe2 = 89.7(1)°	

each layer, there are two crystallographically distinct Fe^{3+} sites (Fe1 and Fe2) which are bridged together to form triangle-based chains, as shown in Fig. 1. These $[Fe_4O_{14}]^{\infty}$ chains extend along the crystallographic b axis and are structurally confined from one another via diamagnetic As^{5+} cations in AsO_4 tetrahedral units along the crystallographic a axis (Fig. 1). Due to the nonmagnetic nature of the As^{5+} cation, the magnetic interactions between adjacent $[Fe_4O_{14}]^{\infty}$ Δ chains via the Fe-O-As-O-Fe connection are expected to be subdominant compared to the interactions within the chains.

A comparison of the refined bonds and angles in $Rb_2Fe_2O(AsO_4)_2$ indicates different interactions occurring between spins on the base (J_{bb} coupling) and between the base-vertex angles (J_{bv}) of the triangles. The Fe1–Fe2 and the Fe2–Fe2 distances are 3.076(1) and 2.895(1), respectively. The bond angles Fe2-O1-Fe2 and Fe2-O2-Fe2 defining the superexchange paths along the base of triangles (J_{bb}) are 97.7(3)° and 89.7(7)°, respectively, while the base-vertex angles (J_{bv}) Fe1-O1-Fe2 and Fe1-O3-Fe2 are 105.9(1)° and 91.5(1)°, respectively.

B. Macroscopic magnetic measurements

Magnetization measurements were performed on single crystals with the b axis (chain direction) aligned parallel and perpendicular to the magnetic field. Due to the small size of the crystals, several specimens were optically comounted on a Kapton tape, as displayed in Fig. 2. Two samples were prepared with total masses of 4.0 and 8.4 mg. The measured magnetization was confirmed to be consistent between the two samples. The temperature dependence of magnetic susceptibility ($\chi = M/H$) measured with an applied field of 100 Oe is shown in Fig. 2. The sharp rise in magnetization data reveals the onset of long-range magnetic order below approximately 25 K. There is strong anisotropy between the two crystal orientations near the transition temperature. The inverse susceptibility (H/M) for temperature well above this temperature is shown in the inset, along with a fit using the Curie-Weiss model, $M/H = C/(T - \Theta_{CW})$. The data are not strictly linear over this wide temperature range. A better fit can be obtained by including a temperature-independent term; however, such a fit returns unreasonable values for the fitting parameters. The observed deviation from Curie-Weiss behavior may indicate some short-ranged or low-dimensional magnetic ordering above the long-ranged ordering transition at 25 K. Using the fit shown in Fig. 2, an effective moment of 6.7(1) μ_B and a Weiss temperature of -510 K are determined. Restricting the fitted range to the more linear region between 250 and 350 K gives an effective moment of 6.3 μ_B and a Weiss temperature of -426 K. These effective moments are somewhat larger than the spin-only value for high spin d^5 of 5.9 μ_B. The large and negative Weiss temperatures indicates strong antiferromagnetic interactions.

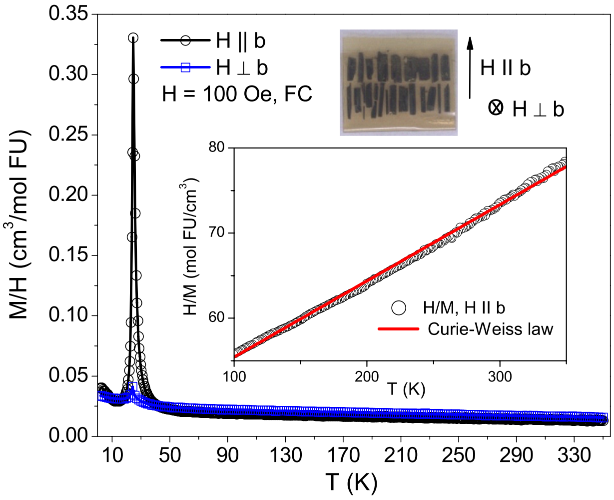

FIG. 2. (Color online) Evolution of the magnetic susceptibility (M/H) as a function of temperature, for $H = 100$ Oe applied parallel and perpendicular to the b axis. The inserted picture displays the single-crystals assembly used in the measurements. Inset: The inverse susceptibility vs temperature above the transition temperature, and a linear (Curie-Weiss) fit.

Additional magnetization measurements were performed near the ordering temperature. Data were collected upon warming from 2 to 50 K in zero-field-cooled (ZFC) and field-cooled (FC) modes. Figure 3 displays the FC results for the four selected fields of 10 Oe, 100 Oe, 1 kOe, and 10 kOe. The temperature dependence changes significantly as the applied field is varied, and the data show strong anisotropy between the two measurement directions at all fields. For H along the direction of the sawtooth chains (the b axis), a sharp cusp, suggesting a canted antiferromagnetic order, is seen at the magnetic ordering transition for $H \leqslant 1$ kOe, while at 10 kOe the susceptibility increases and then saturates upon cooling, similar to the behavior expected at a ferromagnetic transition. For H aligned perpendicular to the b axis, a smaller cusp is seen at all of the fields shown. The qualitative difference between the behavior in the two directions at $H = 10$ kOe is due to a field-induced magnetic transition which occurs at a different field in the different orientations and is discussed in more detail below.

Negative magnetic susceptibilities were observed in some ZFC measurements at low fields. An example is shown in Fig. 4(a), where the magnetization is negative at low temperatures and switches sign abruptly upon warming as the phase transition is approached. This was observed at fields up to 100 Oe and in both orientations of the field. Temperature-induced magnetization reversal phenomena are well known to occur in ferrimagnetic systems with strong magnetic anisotropy displaying a partial cancellation of antiferromagnetically coupled magnetic sublattices with different

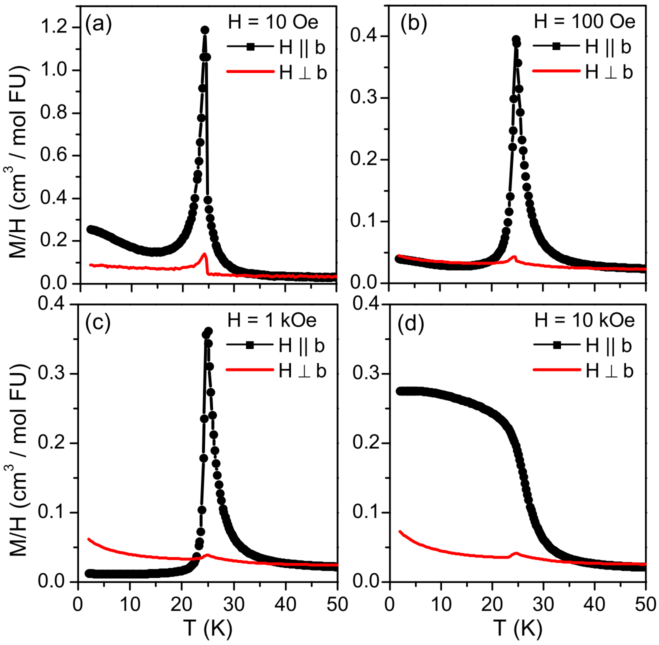

FIG. 3. (Color online) Magnetization curves for coaligned single crystals of $Rb_2Fe_2O(AsO_4)_2$ measured on warming at the indicated fields after field cooling from 50 K. Results are shown for H parallel and perpendicular to the *b* axis along which the sawtooth chain of Fe is oriented.

magnitudes of magnetic moments and/or different temperature dependence of magnetization [17,18]. This scenario is certainly plausible in our system where Fe^{3+} occupies two nonequivalent sites and is exposed to different molecular fields. However, a negative ZFC magnetization curve has also been attributed in some cases to the existence of a small trapped field in the superconducting magnet [19,20]. Such an experimental artifact is likely to occur in some ferromagnetic materials with strong anisotropy and a significant coercive field that can drastically affect the ZFC process. To investigate this possibility, we performed experiments in which we reduced the field to zero from both 10 and −10 kOe using the MPMS "no-overshoot" mode at 50 K, then cooled in "zero field" to 2 K, applied 10 Oe, and then measured upon warming. As discussed in Ref. [19], the sign of the trapped field is opposite in sign when reducing the field to zero from a positive or negative field, and hence a starting field of 10 kOe is expected to generate a small negative trapped field, while −10 kOe will create a small positive trapped field. Our measurements on a Pd reference sample using similar conditions confirm this and indicate the magnitude of the field is several Oe. As apparent in Fig. 4, the ZFC magnetization curves are indeed following the direction of the trapped field in the superconducting magnet. This prompts us to conclude that the observed negative magnetization under the ZFC condition is not a ferrimagnetic effect, but rather a feature induced by the presence of pinned uncompensated spins originated from inhomogeneities [20] or from the antiferromagnetic domain walls [21,22] or slight canting in the antiferromagnetic structure, although no canting could be resolved in the neutron-diffraction results presented below. We note that several ZFC measurements using a field of 10 Oe were also conducted after resetting or quenching the magnet at 50 K. Some of these measurements resulted in behavior such as that shown in Fig. 4(a), and others resulted in behavior such as that shown in Fig. 4(b). This indicates that the residual field, which is expected to be very small (<1 Oe) after resetting the magnet, has unpredictable polarity and that the low-temperature state that is adopted by the material upon cooling through the transition temperature is extremely sensitive to even very small magnetic fields.

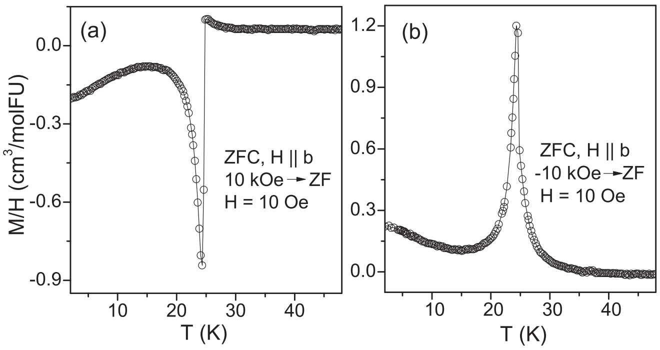

FIG. 4. Zero-field-cooled magnetization curves measured in 10 Oe magnetic field (H ∥ *b*) upon warming from 2 to 50 K after having reduced the field to zero at 50 K from (a) 10 kOe, which leaves a small negative residual field, and (b) −10 kOe, which leaves a small positive residual field.

The isothermal magnetization curves at 2, 10, and 50 K in magnetic fields up to 15 kOe applied along the *b* axis are shown in Fig. 5. The presence of hysteresis in the magnetization data demonstrates the presence of a ferroic component in the high-field magnetic phase. Apart from a hysteresis separating the ascending and descending branches, there is a readily noticeable stepwise magnetic behavior. The metamagnetic transition occurs near 3 kOe at $T = 2$ K and shifts to

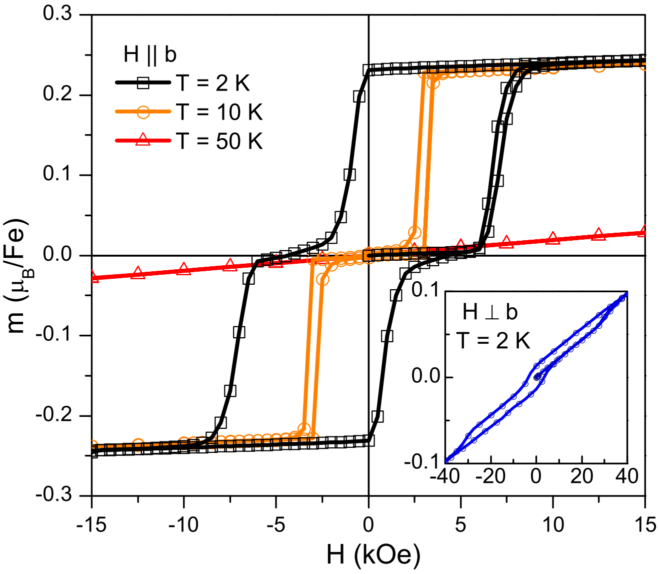

FIG. 5. (Color online) Magnetic field dependence of magnetization for oriented single crystals of $Rb_2Fe_2O(AsO_4)_2$ with H ∥ *b* at four different temperatures. Inset: The isothermal magnetization curve at 2 K for H ⊥ *b*.

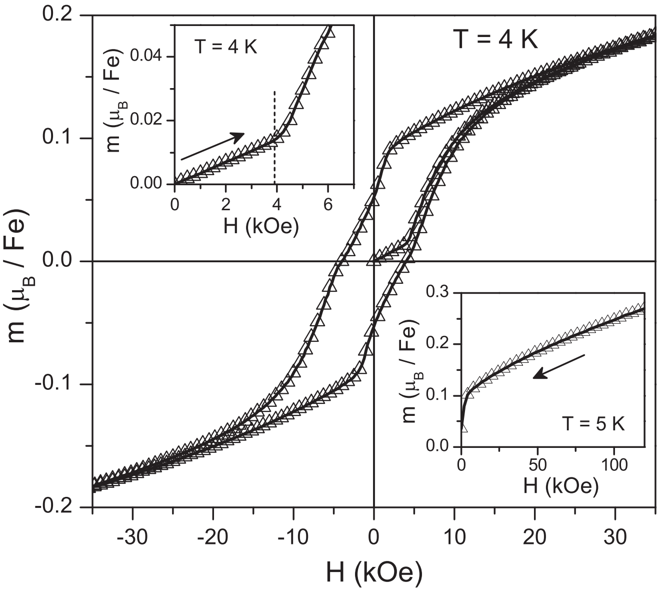

FIG. 6. Isothermal magnetization data measured on a compacted powder sample at $T = 4$ K. Upper inset: A blow up of the region near the metamagnetic transition (≈4 kOe). Lower inset: The magnetization data measured upon reducing the field from 120 kOe at 5 K.

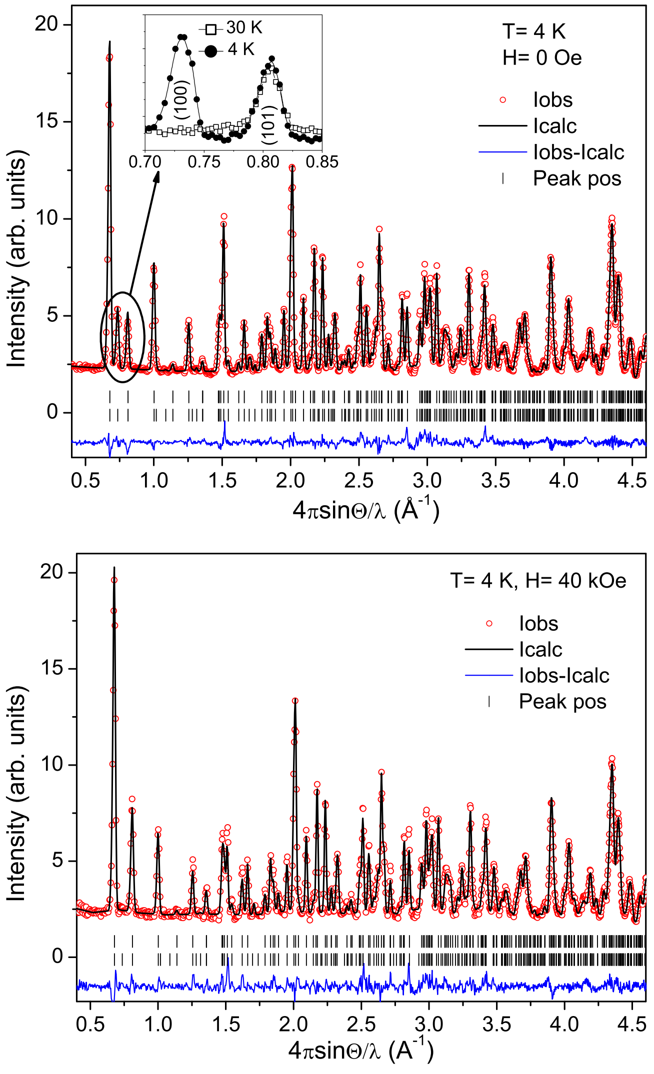

FIG. 7. (Color online) Upper panel: Rietveld plot of neutron powder diffraction data collected at 4 K in zero magnetic field. Inset: A comparison of the low-Q data, near the (100) magnetic peak, measured at 4 and 30 K. Lower panel: Rietveld plot of neutron data measured at 4 K in magnetic field of 40 kOe.

6 kOe at $T = 10$ K. When the field is applied perpendicular to the b axis, the metamagnetic phase transition occurs at a much higher field of 30 kOe, at $T = 2$ K (as shown in the inset of Fig. 5). As expected, the magnetization measured on a compacted powder sample shows a more gradual field transition, arising at approximately 4 kOe at a temperature of 4 K (see Fig. 6). It is also worth noting that the magnetization curves do not reach the full saturation even for the highest applied external fields of 120 kOe. The largest absolute value of the magnetization, of about 0.3 μ_B/Fe, is smaller by over an order of magnitude than the predicted value corresponding to a parallel alignment of the Fe^{3+} magnetic moments ($gS = 5\ \mu_B$).

C. Neutron diffraction

1. Measurements in zero magnetic field

Neutron-diffraction patterns collected in the paramagnetic state at 40 K are well described by the structural model described in the previous section. Upon cooling below 25 K, magnetic Bragg peaks [e.g., (100), (102)] start to appear at low angles (see Fig. 7), indicating a transition to an antiferromagnetic long-range order. The evolution with temperature of (100) magnetic peak intensity is shown in Fig. 8 (upper panel). Near the transition temperature, the order parameter follows a power-law behavior.

Representational analysis was conducted to determine the symmetry-allowed magnetic structures that can result from a second-order magnetic phase transition given the crystal structure and the propagation vector $k = (0,0,0)$ of the magnetic ordering. These calculations were carried out using the program SARA*h*-REPRESENTATIONAL ANALYSIS [23]. There are eight possible irreducible representations (IRs) associated with the *Pnma* space group and $k = (0,0,0)$. The decomposition of the magnetic representation for the Fe1 site (0.715,0.25,0.565) is $\Gamma_{\rm Mag} = 1\Gamma_1^1 + 2\Gamma_2^1 + 2\Gamma_3^1 + 1\Gamma_4^1 + 1\Gamma_5^1 + 2\Gamma_6^1 + 2\Gamma_7^1 + 1\Gamma_8^1$, while for the Fe2 site (0,0,0.5), it is $\Gamma_{\rm Mag} = 3\Gamma_1^1 + 0\Gamma_2^1 + 3\Gamma_3^1 + 0\Gamma_4^1 + 3\Gamma_5^1 + 0\Gamma_6^1 + 3\Gamma_7^1 + 0\Gamma_8^1$. The labeling of the IRs follows the scheme used by Kovalev [24]. Table III presents only two of the representations ($\Gamma1$, $\Gamma5$) that are relevant for our discussion here.

The 4 K diffraction data was fit by a magnetic structure model based on the representation Γ_1, defined in Table III. Γ_1 representation is equivalent to the Shubnikov magnetic space group *Pnma*. Within this model, the Fe1 moments are constrained to lie along the b-axis direction and are ferromagnetically coupled to each other inside the chain. In contrast, the Fe2 moments have components in all three coordinate directions and form an undulating pattern with the relative angles between neighboring spins of approximately 60°. The spin canting occurs in such a way that they remain mostly confined to the plane of the sawtooth chain. The

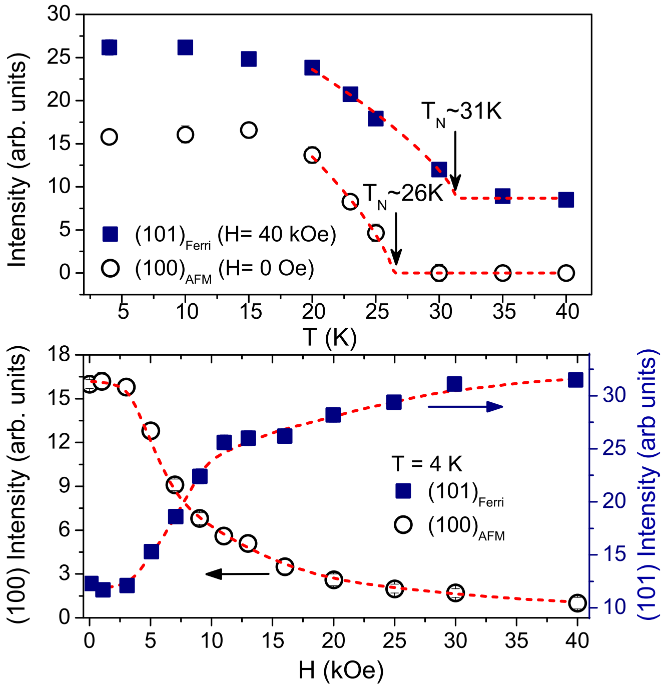

FIG. 8. (Color online) Upper panel: Temperature dependence of the (100) and (101) peak intensities measured in zero magnetic field and 40 kOe, respectively. The lines represent a guide to the eye indicating power-law behavior. Lower panel: Variation with magnetic field of the (100) and (101) magnetic peaks at 4 K. The dashed line is a guide to the eye. The vanishing of (100) reflection at the expense of (101) magnetic peak is caused by an induced transition from antiferromagnetic to ferrimagnetic state.

projection along the chain axis of the Fe2 moment is oriented in opposite direction to the Fe1 moment, thus producing a nonzero net moment. The polarity of the chains alternates along the c-axis direction, giving an overall antiferromagnetic arrangement. A stereographic view of the magnetic structure is illustrated in Fig. 9(a).

The refined magnitudes of the ordered moments for the Fe1 and Fe2 sites are 3.64(6) and 3.19(8) μ_B, respectively. The projections of the Fe2 magnetic moment on the three axes of coordinates are $\mu_a = 1.19(8)\ \mu_B$, $\mu_b = 2.88(4)\ \mu_B$, and $\mu_c = 0.68\ (9)\ \mu_B$. The refined values are significantly lower than those expected for the Fe^{3+} ions with the effective spin $S = 5/2$. Considering the high value of the frustration parameter $f = |\Theta_{CW}|/T_N$ of approximately 18, one can infer that the reduced static magnetic moment is due to the presence of spin frustration. The frustration is reasonably expected in this system due to competing superexchange interactions within the triangular chains. Furthermore, the noncollinear spin arrangement is reminiscent of the predicted noncollinear spin configurations in the triangular-lattice Heisenberg antiferromagnet, where the frustration of the three nearest-neighbor spins on a triangular plaquette is resolved by a 120° rotation of neighboring spins [25].

Perhaps the most important aspect that needs to be emphasized here is the fully compensated character of the magnetic structure, which makes the magnetization reversal process observed in the ZFC magnetization data difficult to comprehend. The ferrimagneticlike response has previously been observed only in a handful of antiferromagnetic compounds where a weak ferromagnetic moment is due to the tilting of sublattice magnetizations [26–29]. One of the mechanisms that has been proposed to explain the magnetization reversal in antiferromagnets relies on the competition between single-ion anisotropy and the DzyaloshinskyMoriya (DM) interaction. For our system, the antisymmetric DM exchange coupling can exist between the magnetically ordered Fe2 ions located at the 4b site of $Pnma$, and the magnetic spin corresponding to that site has indeed been determined to be canted. However, because the chains are antiferromagnetically coupled, any ferromagnetic component due to canting is compensated by the nearest-neighbor chain. These results come to confirm our conjecture in the previous section that the negative magnetization is not an inherent ferrimagnetic feature, but likely an effect of an uncompensated magnetization originating from antiferromagnetic domain walls or from other magnetic inhomogeneities present in the sample.

TABLE III. Basis vectors (BVs) of the IRs Γ_1 and Γ_5, of the space group $Pnma$ with $k = (0,0,0)$. The equivalent Fe1 atoms of the nonprimitive basis are defined according to 1: (0.715,0.25,0.565), 2: (0.215,0.25,0.934), 3: (0.284,0.75,0.434), and 4: (0.784,0.75,0.065). The Fe2 atoms are defined as follows: 1: (0,0,0.5), 2: (0.5,0.5,0), 3: (0,0.5,0.5), and 4: (0.5,0,0).

			Fe1			Fe2		
IR	BV	Atom	$m_{\parallel a}$	$m_{\parallel b}$	$m_{\parallel c}$	$m_{\parallel a}$	$m_{\parallel b}$	$m_{\parallel c}$
Γ_1	ψ_1	1	0	1	0	0	1	0
		2	0	−1	0	0	−1	0
		3	0	1	0	0	1	0
		4	0	−1	0	0	−1	0
	ψ_2	1				1	0	0
		2				1	0	0
		3				−1	0	0
		4				−1	0	0
	ψ_3	1				0	0	1
		2				0	0	−1
		3				0	0	−1
		4				0	0	1
Γ_5	ψ_4	1	0	1	0	0	1	0
		2	0	1	0	0	1	0
		3	0	1	0	0	1	0
		4	0	1	0	0	1	0
	ψ_5	1				1	0	0
		2				−1	0	0
		3				−1	0	0
		4				1	0	0
	ψ_6	1				0	0	1
		2				0	0	1
		3				0	0	−1
		4				0	0	−1

2. *Measurements in external magnetic fields*

To understand the effect of magnetic field on the magnetic structure of $Rb_2Fe_2O(AsO_4)_2$, a polycrystalline sample in the

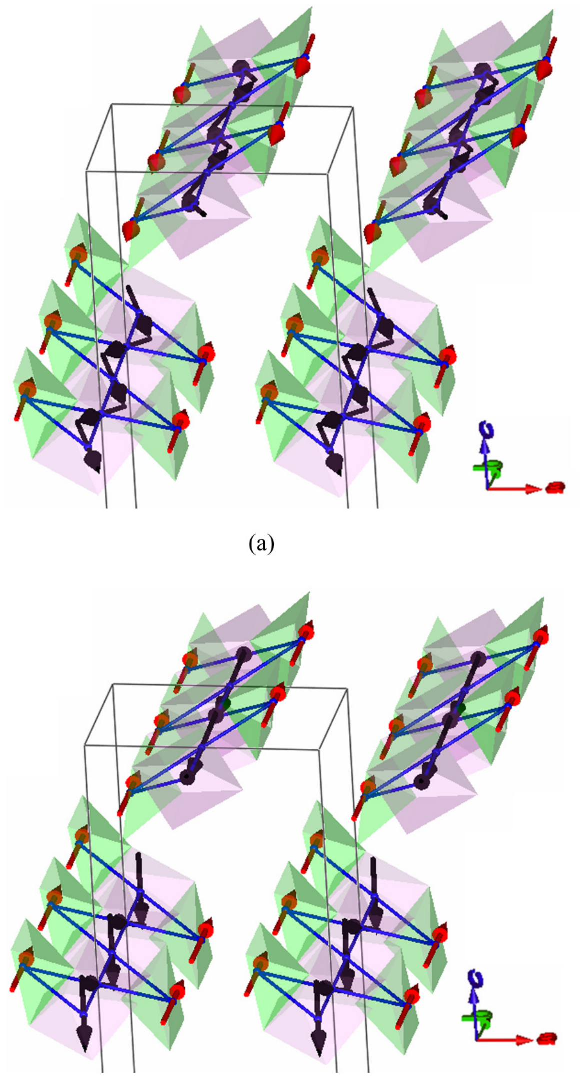

(a)

(b)

FIG. 9. (Color online) (a) Schematic view of the magnetic structure of $Rb_2Fe_2O(AsO_4)_2$ at 4 K and zero magnetic field. The Fe1 magnetic moments are collinear with the *b* axis, while the Fe2 moments are forming undulating patterns, running in opposite direction with respect to the Fe1 moments. The ferrimagnetic chains are coupled antiferromagnetically to neighboring chains in the *c*-axis direction. (b) Magnetic structure at 4 K and applied magnetic filed of 40 kOe. In contrast to the zero-field magnetic order, the polarity of the ferrimagnetic chains remains the same throughout the lattice, yielding an overall ferrimagnetic ordering.

form of pressed pellets has been measured under different magnetic fields up to 40 kOe. The diffraction data measured at 4 K reveal a progressive decrease in the amplitude of (100) magnetic peak with increasing the applied magnetic field and, at the same time, an increase in intensity of the (101) peak. The change in peaks intensities only manifests at low-momentum transfer (Q), in accordance with the Fe^{3+} magnetic form factor. The fact that the high-Q reflections are not affected by the magnetic field gives assurance that the sample grains do not realign in the direction of the field. As displayed in Fig. 8 (lower panel), the (100) peak intensity starts to decrease just above 3 kOe and it nearly vanished at 40 kOe. The (101) peak follows a very similar trend to that seen for the isothermal magnetization curve measured for the powder sample in the magnetically ordered state at 4 K, shown in Fig. 6. The intensity of the (101) peak has also been monitored as a function of temperature in a constant magnetic field of 40 kOe. The order parameter versus temperature shown in Fig. 8 (upper panel) follows a power-law dependence, similar as that observed for the (100) peak in zero magnetic field.

Rietveld refinement has been performed using the diffraction data collected at 40 kOe and 4 K, and the fit result is presented in Fig. 7. The magnetic scattering has been well reproduced by a ferrimagnetic model based on the irreducible representation Γ_5 given in Table III. This representation is equivalent to the Shubnikov magnetic space group $Pn'ma'$. In this magnetic state, all chains exhibit the same polarity, with all symmetry-equivalent Fe ions having the *b*-axis component of magnetic moment aligned in the same direction. On the other hand, Fe1 and Fe2 sublattices maintain opposite magnetizations while not compensating each other. Another effect of the magnetic field is the change in the canting direction of Fe2 spins with respect to the local plane of the sawtooth chain. The spins rotate around the *b* axis from an in-plane canting to an out-of-plane canting. The relative angle between Fe2 and Fe1 moments remains close to 120°. The high-field magnetic structure is shown in Fig. 9(b).

The magnitude of the ordered magnetic moments at 40 kOe is determined to be very close to that observed for the antiferromagnetic state in zero magnetic field. The refined Fe1 moment is 3.5(1) μ_B, while the amplitude of the Fe2 moment is 3.1(1) μ_B with the three axes components $\mu_a = 0.5(1)$ μ_B, $\mu_b = 2.76(6)$ μ_B, and $\mu_c = 1.3(1)$ μ_B. These values appear to rule out the possibility that the external magnetic field may polarize additional disordered Fe spins into the ordered state described above. On the other hand, the net magnetization resulting from such amplitudes is about 0.37 μ_B per Fe^{3+}, which is reasonably consistent with what has been determined from magnetization measurements (see Figs. 5 and 6). Interestingly, the magnetization data shown in Fig. 5 suggest that at sufficiently low temperatures, the field-induced ferrimagnetic state can be maintained even after reducing the field back to zero.

It appears that the metamagnetic transition corresponds to the transition from the antiferromagnetic to ferrimagnetic state where all magnetic couplings between the adjacent sawtooth chain become exclusively ferromagnetic, while the intrachain exchange interactions remain nearly unaltered. The field-induced ferrimagnetic ordering provides an interesting insight into the tendency of the system to produce a net ferromagnetic component, and opens up the question of whether a local ferrimagnetic cluster may start to form within the antiferromagnetic host even at very low magnetic fields. The contribution to the scattering of such weak uncompensated magnetic order could be well below the detection limit of our neutron scattering measurements. Magnetic clustering could plausibly explain the observed negative magnetization, but it implies the existence of inhomogeneities in the sample. Note that in our case, the inhomogeneities would likely have their origin in oxygen vacancies, which could not be either confirmed or ruled out by our structural refinement. As mentioned before, the uncompensated spins might also result from antiferromagnetic domain walls, as demonstrated in the case of the $HoMnO_3$ multiferroic system by means of polarized small-angle neutron scattering experiments [21].

IV. SUMMARY

The magnetic properties of oxy-arsenate $Rb_2Fe_2O(AsO_4)_2$ have been studied by means of magnetization and neutron powder diffraction measurements. The system structure consists of triangle-based magnetic chains made of $S = 5/2$ Fe^{3+} ions occupying two crystallographically distinct tetrahedral sites (Fe1 and Fe2). Magnetization measurements indicate a complex magnetic behavior with a temperature-induced magnetization reversal at low magnetic fields, and a step-like metamagnetic transition. Neutron-diffraction experiments performed in zero magnetic field reveal an antiferromagnetic long-range magnetic order below the Néel temperature of about 25 K. The magnetic structure consists of ferrimagnetic sawtooth chains which are mutually compensating each other along the c direction. Within each chain, the Fe1 moments are collinear lying along the b direction, while the Fe2 moments are reversely canted by approximately 30°, forming a zigzag pattern. A reduced static magnetic moment of Fe has been attributed to a magnetic frustration caused by the triangle geometry. Neutron data collected under externally applied magnetic field reveal a transition from an antiferromagnetic to a ferrimagnetic state. In the ferrimagnetic state, the individual chains remain ferrimagnetic with similar spin topology, but their coupling becomes exclusively ferromagnetic. The ferrimagnetic ordering at magnetic fields greater than 3 kOe cannot be invoked to explain the negative ZFC magnetization observed in the macroscopic study. Instead, the present data suggest that the negative magnetization could be an effect of a phase-segregated state with ferrimagnetic inclusions or of an uncompensated magnetization arising within antiferromagnetic domain walls. On the basis of our results, the sawtoothlike lattice model displayed by the $Rb_2Fe_2O(AsO_4)_2$ system deserves further experimental and theoretical investigations to fully understand its magnetic behavior. While the magnetic phase-segregation antiferromagnetic domain walls are, at present, only hypothetical scenarios, future polarized neutron scattering experiments able to provide increased sensitivity to weak ferromagnetism may shed light on the origin of the negative-magnetization phenomenon.

ACKNOWLEDGMENTS

Work at the Oak Ridge National Laboratory was sponsored by the Scientific User Facilities Division (neutron diffraction) and Materials Sciences and Engineering Division (magnetization measurements), Office of Basic Energy Sciences, US Department of Energy (DOE). The authors acknowledge the financial support from the National Science Foundation: Grants No. DMR-0706426, No. CHE-9808165, and No. CHE-9808044. L.D.S. and D.S.'s travel to ORNL was supported by the US DOE through the EPSCoR Grant No. DE-FG02-08ER46528.

---

[1] S.-J. Hwu, Chem. Mater. **10**, 2846 (1998).

[2] W. L. Qeen, S.-J. Hwu, and L. Wang, Angew. Chem. Int. Ed. **46**, 5344 (2007); J. P. West, S.-J. Hwu and W. L. Queen, Inorg. Chem. **48**, 8439 (2009); J. P. West, W. L. Queen, S. J. Hwu, and K. E. Michaux, Angew. Chem. Int. Ed. **50**, 3780 (2011).

[3] C. Wurm, M. Morcrette, G. Rousse, L. Dupont, and C. Masquelier, Chem. Mater. **14**, 2701 (2002).

[4] Y. Uebou, S. Okada, M. Egashira, and J.-I. Yamaki, Solid State Ionics **148**, 323 (2002).

[5] C. Masquelier, A. K. Padhi, K. S. Nanjundaswany, and J. B. Goodenough, J. Solid State Chem. **135**, 228 (1998).

[6] A. K. Padhi, K. S. Nanjunclaswamy, C. Masquelier, S. Okada, and J. B. Gooclenough, J. Electrochem. Soc. **144**, 1609 (1997).

[7] D. Sen, B. S. Shastry, R. E. Walstedt, and R. Cava, Phys. Rev. B **53**, 6401 (1996).

[8] T. Nakamura and K. Kubo, Phys. Rev. B **53**, 6393 (1996).

[9] S. A. Blundell and M. D. Nunez Regueiro, Eur. Phys. J. B **31**, 453 (2003).

[10] G. Van Tendeloo, O. Garlea, C. Darie, C. Bougerol-Chaillout, and P. Bordet, J. Solid State Chem. **156**, 428 (2001); V. Garlea, C. Darie, O. Isnard, and P. Bordet, Solid State Sci. **8**, 457 (2005).

[11] H. Kikuchi, Y. Fujii, D. Takahashi, M. Azuma, Y. Shimakawa, T. Taniguchi, A. Matsuo, and K. Kindo, J. Phys.: Conf. Ser. **320**, 012045 (2011).

[12] G. C. Lau, B. G. Ueland, R. S. Freitas, M. L. Dahlberg, P. Schiffer, and R. J. Cava, Phys. Rev. B **73**, 012413 (2006).

[13] R.-S. Chang, S.-L. Wang, and K.-H. Lii, Inorg. Chem. **36**, 3410 (1997).

[14] G. M. Sheldrick, C. Kruger, and R. Goddard, Crystallogr. Comput. **3**, 175 (1985); Computer code SHELXTL 6.12 (Bruker Analytical X-ray Systems Inc., Madison, WI, 2001).

[15] V. O. Garlea, B. C. Chakoumakos, S. A. Moore, G. B. Taylor, T. Chae, R. G. Maples, R. A. Riedel, G. W. Lynn, and D. L. Selby, Appl. Phys. A **99**, 531 (2010).

[16] J. Rodriguez-Carvajal, Physica B **192**, 55 (1993); program available at www.ill.fr/dif/Soft/fp/ (unpublished).

[17] L. Neel, Ann. Phys. **3**, 137 (1948).

[18] N. Menyuk, K. Dwight, and D. G. Wickham, Phys. Rev. Lett. **41**, 119 (1960).

[19] N. Kumar and A. Sundaresan, Solid State Commun. **150**, 1162 (2010).

[20] A. A. Belik, Inorg. Chem. **52**, 8529 (2013).

[21] B. G. Ueland, J. W. Lynn, M. Laver, Y. J. Choi, and S.-W. Cheong, Phys. Rev. Lett. **104**, 147204 (2010).

[22] M. Bode, E. Y. Vedmedenko, K. von Bergmann, A. Kubetzka, P. Ferriani, S. Heinze, and R. Wiesendanger, Nat. Mat. **5**, 477 (2006).

[23] A. S. Wills, Physica B **276**, 680 (2000); program available from www.ccp14.ac.uk (unpublished).

[24] O. V. Kovalev, *Representations of the Crystallographic Space Groups*, 2nd ed. (Gordon and Breach Science, Switzerland, 1993).

[25] L. Capriotti, A. E. Trumper, and S. Sorella, Phys. Rev. Lett. **82**, 3899 (1999).

[26] H. Kageyama, D. I. Khomskii, R. Z. Levitin, M. M. Markina, T. Okuyama, T. Uchimoto, and A. N. Vasil'ev, J. Magn. Magn. Mater. **262**, 445 (2003).

[27] R. P. Singh and C. V. Tomy, J. Phys.: Condens. Matter **20**, 235209 (2008).

[28] Y. Ren, T. T. M. Palstra, D. I. Khomskii, A. A. Nugroho, A. A. Menovsky, and G. A. Sawatzky, Phys. Rev. B **62**, 6577 (2000).

[29] Y. Kimishima, Y. Chiyanagi, K. Shimizu, and T. Mizuno, J. Magn. Magn. Mater. **210**, 244 (2000).